Structural, and magnetic properties of $Ni_{0.4-x}Co_xCu_{0.2}Zn_{0.4}Fe_2O_4$ ferrite nanoparticles

K. Jayadev[1], N. Murali[2], K. Samatha[1]

[1]Department of Physics, Andhra University, Visakhapatnam, Andhra Pradesh

[2]Department of Engineering Physics, AUCE (A)Andhra University, Visakhapatnam, Andhra Pradesh

Abstract: $Ni_{0.4-x}Co_xCu_2Zn_{0.4}Fe_2O_4$ (x = 0, 0.1, and 0.2) were produced by a sol-gel method involving auto-combustion. X-ray Diffraction (XRD), Field effect scanning electron microscopy (FESEM), Fourier Transform Infrared (FTIR) Spectroscopy, and Vibrating Sample Magnetometer (VSM) were used for determining the structural, electrical, and magnetic properties of these ferrites respectively. The result of the lattice constant, crystallite size, particle size, bond lengths, magnetization, and coercivity shows these spinel materials to be highly significant in everyday life.

Keywords: NiCuZn nano ferrites, XRD, Saturation magnetization.

1. Introduction

Ferrites nanoparticles and their composites are famous due to their unusual but useful electric, magnetic, and adsorption properties used in recording devices, absorber, microwave device applications, cationic dyes, drug delivery, MRI applications, and sensors [1-3]. The ferrite nanoparticles with the general formula AB_2O_4 have a spinel structure [4]. Cobalt ferrite $CoFe_2O_4$ is partially inverted spinel structured hard ferrite. More Co^{2+} ions in the octahedral site [5] and Fe^{3+} ions are tetrahedral sites. The magnetic moment of Fe^{3+} ions is $5\mu_B$ and $3\mu_B$, respectively [5]. The cation distribution in different sites plays an important role in the property of spinel. The interchange (A to B and half from B to A) of cations in the two interstitial sites gives rise to inverted spinel. The proportion of interchange determines the resulting material properties [6]. The partial substitution of Zinc in cobalt ferrite can produce sufficient positive changes in the properties of spinel structure like magnetic properties and electrical resistivity for sensors and actuator applications [7]. Some of the recent approaches like microemulsion, co-precipitation, ceramic, hydrothermal, sol-gel methods, etc. [8-10] help a lot in the synthesis of the material of our interest. The easy and faster sol-gel method is used for ultrafine particles at room temperature.

In this work, Co substituted $Ni_{0.4-x}Co_xCu_2Zn_{0.4}Fe_2O_4$ (x = 0, 0.1, and 0.2) ferrites are prepared by sol-gel auto combustion method, and their different properties are studied using XRD, FESEM, FTIR, and VSM etc.

2. Experimental Techniques

The starting elements were analytically graded of highest purity mixed with citric acid in a 1:1M ratio. When annealed at low temperature, the mixture gives rise to the single-phase ferrites, neutralized with ammonia. The neutral solution is made clear with the help of deionized water and heated to 150 ºC until the

formation of gel is converted into ash after the combustion and hence powdered. The powder is again sintered at 800 ˚C for 4 hours, and pallets were prepared for characterization. The citric acid is used to homogenize the solution, and PVA as a binder for the pallet formation is used to study electrical properties.

The radiation of Cu Kα with 1.5406 Å wavelength is incorporated in Rigaku Miniflex II XRD for the structural, TESCAN- MIRA II LMH SEM for the morphological, EDX, Inca Oxford for compositional, FTIR for a functional group, EZ-VSM for room temperature magnetic properties, and two probe method for the study of DC resistivity of the samples.

3. RESULTS AND DISCUSSIONS

3.1 XRD Studies

The XRD plots of different Co substituted $Ni_{0.4-x}Co_xCu_2Zn_{0.4}Fe_2O_4$ (x = 0, 0.1, and 0.2) samples are shown in Figure 1. The structure of the sample is found to be a cubic spinel structure according to the JCPDS card No.48- 0489. The lattice constant 'a' is determined with the following relation [11].

$$\mathbf{a = d_{hkl}\sqrt{h^2 + k^2 + l^2}}$$

where d_{hkl} is more interplane spacing for given hkl planes and is calculated by Bragg's law, the plot of intensity against the diffracting angle (2) for different concentrations of ferrite nanoparticles (NPs). The highest intensity (311) peak indicates the crystallite size appropriate orientation to measure its degree of crystalline nature to find the average crystallite size of all samples [9]. Debye-Scherer's formula gives the average size of the crystallite size [12].

$$D_{311} = \frac{0.9\lambda}{\beta cos\theta}$$

where D_{311}, λ, β and θ are volume-averaged crystallite size, the wavelength of X-ray (1.5406Å), full width at half maximum of (311) peak and diffraction angle respectively.

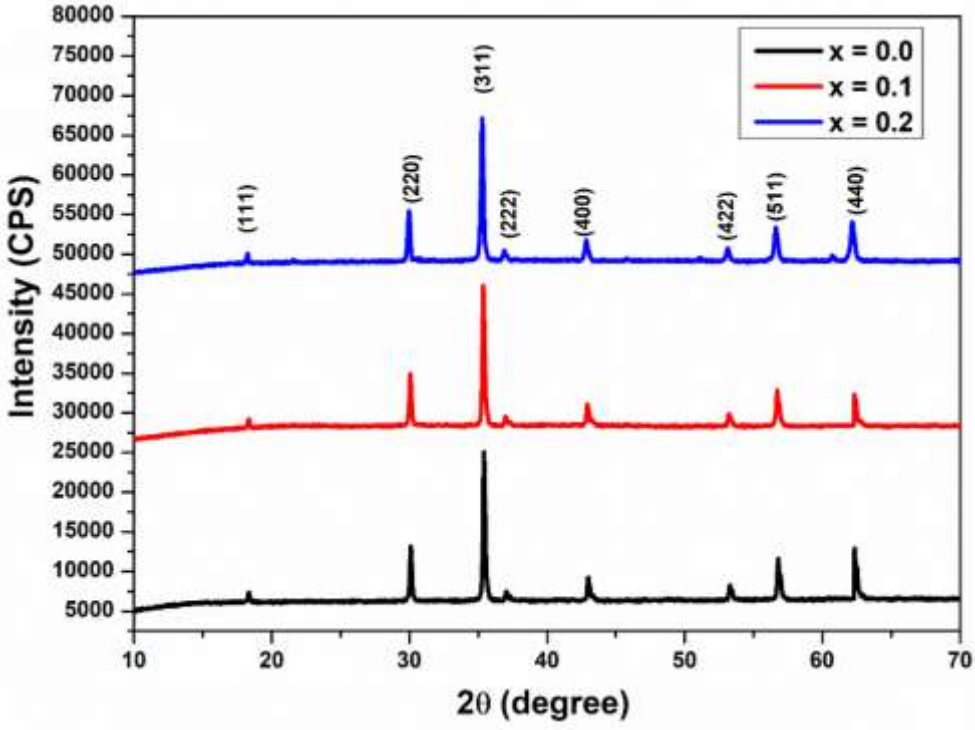

Figure 4.1: X-ray diffraction patterns of Co substituted NiCuZn ferrite

The crystallite size, lattice parameters, and cell volume of the composition are listed in Table 1. The increasing-decreasing pattern of crystallite size is due to the lattice strain produced in the synthesis process. As the number of disorders decreases, the size of the crystal increases. In contrast, the lattice constant is found to increase with increasing Co content. Crystallite size initially increases with Co concentration up to x = 0.2. Decrease inthe lattice constant (a) due to a smaller ionic radius of Co^{2+} (0.58 Å) replacing Ni^{2+} (0.69 Å) ions [12]. The obtained value of the lattice parameter of the base (x = 0) sample is 8.3237 Å. The lattice compression may also be due to the partial oxidation of Ni^{2+} to Ni^{3+}, Co^{2+} to Co^{3+}[13]. The zinc loss and gain are usually credited to the surface, forming a common boundary structure between surfaces with a more volume fraction. The lattice constant is more significant in the smaller size of the nanoparticle. The diffraction peak width (β) is inversely proportional to the crystallite size from Scherer's formula. The increase in the lattice parameter expands the volume of the unit cell accordingly.

Table 4.1: Lattice parameters of Co substituted NiCuZn ferrite

Concentration (x)	Lattice constant a (Å)	Crystallite size (nm)	Space Group
0.0	8.3237	32.24	Fd-3m
0.1	8.3908	26.24	Fd-3m
0.2	8.3799	25.84	Fd-3m

3.2 Field-Effect Scanning Electron Microscope (FESEM) studies

The images obtained from FESEM showing morphology and microstructure of the $Ni_{0.4-x}Co_xCu_2Zn_{0.4}Fe_2O_4$ (x = 0, 0.1, and 0.2) samples are shown in Figures 2. Initially, the molecules seem more or less round with some agglomeration between them. A sol-gel burning strategy obtains the fine-grained microstructure of all mixed ferrites [14]. The porosity and agglomeration diminish with Co content which is usual in ceramic materials [15]. The average grain size determined from the field effect scanning electron microscopy technique is of the order of 70 to 90 nm.

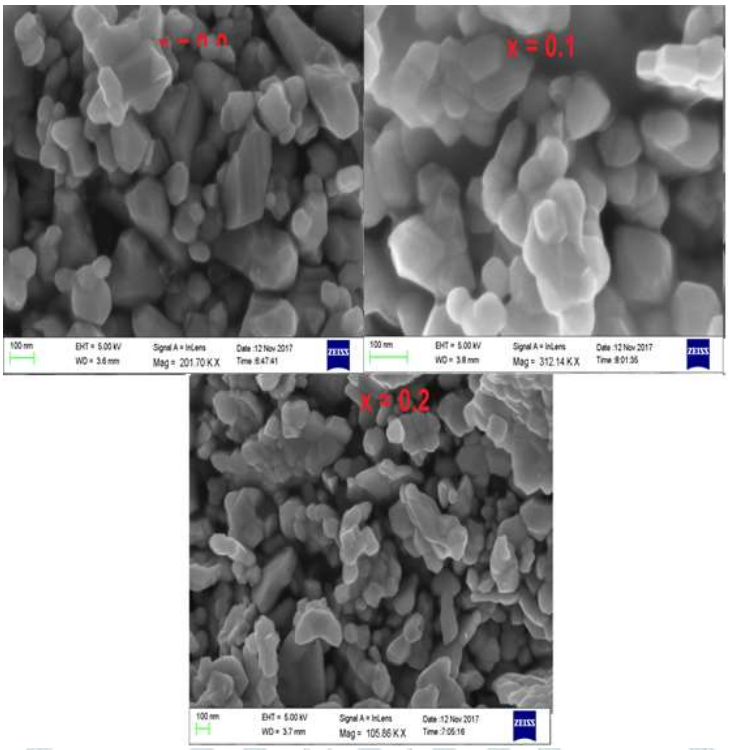

Figure 2: FESEM images for of Co substituted NiCuZn ferrite

3.3 Fourier Transformed Infrared (FTIR) Spectroscopy studies

Normally, the spinel ferrites $Ni_{0.4-x}Co_xCu_2Zn_{0.4}Fe_2O_4$ (x = 0, 0.1, and 0.2) have a wavenumber range from 400-600 cm^{-1}**.** Their mean distance of anion oxygen and metal cations in the tetrahedral and octahedral sites are found to be 1.89A^o and 1.99A^o in respectively. This is the main reason for having two absorption bands for a ferrite at the two sites [16]. As a result, the center of frequency shifted towards the high-frequency site. This confirms the occupancy of Co^{2+} in the octahedral site. There is also the possibility of migration of some Co^{2+} from B to A in this particular concentration range. The values of the two absorption bands for the mentioned composition for different concentrations of Co are listed in table 2, and their respective IR spectra are shown in figure 3 respectively. The general trend of transmittance is increasing with the concentration. All the compositions are mixed ferrites. The octahedral frequency is below 400 cm^{-1}, which may be due to the decrease in site radius and vibration with the increment in non-magnetic Co^{2+} concentration.

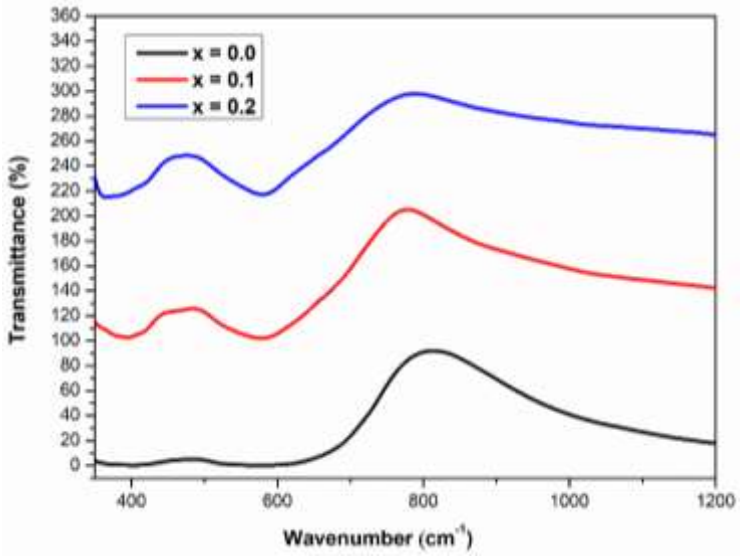

Figure 4: Infrared spectra of Co substituted NiCuZn ferrite

Table 2: Absorption bands of Co substituted NiCuZn ferrite

Concentration (x)	Tetrahedral υ_1(cm^{-1})	Octahedral υ_2(cm^{-1})
0.0	402.15	580.44
0.1	406.62	587.09
0.2	410.17	598.37

4.3.4 Magnetic properties

Ferrites have antimagnetic moments with unequal magnitudes. As a result, they have a large value of spontaneous magnetization. The exchange integral, depending on interatomic distance, is negative for ferrite. This indirect exchange interaction through oxygen ions limits the easy flow of electrons. So, ferrites have high resistivity [17]. The hysteresis curves of our respective samples are as shown in figure 4. They give the values of coercivity (Hc), saturation magnetization (Ms), etc., important for their magnetic properties from coercive field and saturation magnetization variation with Mg substituted NiCuZn. The values of Ms and Hc are listed in Table 3 [18]. Saturation magnetization (M_s) decreases from 89.93 (x=0.0) to 46.32 emu/g for x=0.2 with increasing Co in content. H_c increases initially 45.36 Oe (x=0.0), and then decreases to 51.48 Oe (x=0.2).

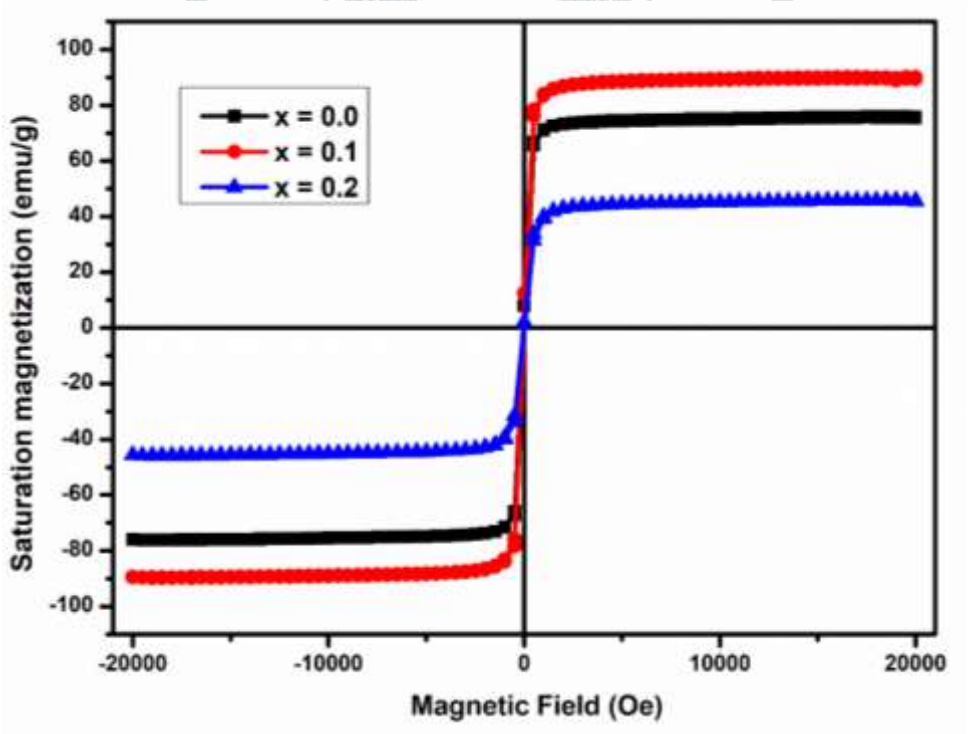

Figure 4: Hysteresis curve of Co substituted NiCuZn ferrite

Table 3: M_s and H_c of Co substituted NiCuZn ferrite

Concentration (x)	M_s (emu/g)	H_c (Oe)
0.0	89.93	45.36
0.1	69.39	53.45
0.2	46.32	51.48

The substitution of Fe^{3+} by Co^{2+} ions at the tetrahedral site, according to the AB-BA exchange interaction effect, increased the total magnetization of the sample. The magnetic ordering in B sublattice is of uniform triangular type. In a semi-disordered system, ferrite, sudden tilting, or overturning effect (canting) in magnetic moments decreases the magnetization. M_A and M_B represent the magnetic saturation at tetrahedral and octahedral sites. The difference in the magnetic moments in the two sites gives a net magnetic moment

$$Ms= |M_A - M_B|.$$

Moreover, the coercivity decreases with the concentration of Co. Ms depends on size if the number of atoms on the surface is remarkable to the total number of the sample volume. The lower value of M_s indicates the surface effect that makes the magnetic moments non-collinear on the surface, ferrimagnetically aligned spin [19].

From table 3, M_s increases up to ($x \leq 0.15$) and then decreases with Co^{2+} concentration. This is due to the distribution of cations and exchange interaction. On adding Co substituted $Ni_{0.4-x}Co_xCu_2Zn_{0.4}Fe_2O_4$ (x = 0, 0.1, and 0.2) they exchange few magnetic ions Fe^{3+} and Ni^{2+} in B- site increases AB interaction that interrupts the antiparallel spin at B site resulting from the increase in total magnetization [20]. A similar phenomenon occurs on the A site. According to Weiss's molecular field theory, the A-B and B-A interaction dominate the A-A and B-B interaction, resulting in the hysteresis loop [21].

4.4 CONCLUSIONS

Sol-gel auto-combustion method is utilized to fabricate nanocrystalline Co substituted $Ni_{0.4-x}Co_xCu_2Zn_{0.4}Fe_2O_4$ (x = 0, 0.1, and 0.2) ferrite NPs. The structure of the ferrite shown by the X-ray diffraction is single phase cubic spinel. The increasing-decreasing pattern of crystallite size is due to the lattice strain produced in the process of synthesis. Sintering decreases the lattice defects and involved strain but facilitates the crystals' coalition increasing in particle size. FESEM reveals microstructural growth along with heat action. The FTIR spectrum exhibits a prominent ferrite microstructure andthe major impact of the mixture of ingredients. The magnetic measurements show that magnetization reduces and coercivity enhances as the composition x = 0.0.

References

[1] Yu S, Wu G, Gu X, Wang J, Wang Y, Gao H, et al. Colloids Surf, 103 (2013) 15–22.

[2] Tejabhiram Y, Pradeep R, Helen AT, Gopalakrishnan C, Ramasamy C. Mater Res Bull 2014;60:778–82.

[3] Jha DK, Shameem M, Patel AB, Kostka A, Schneider P, Deb AEP. Mater Lett 2013;95:186–9.

[4] Kenouche S, Larionova J, Bezzi N, Guari Y, Bertin N, Zanca M, et al. Powder Technol 2014;255:60–5.

[5] A. Ramakrishna, N. Murali, Tulu Wegayehu Mammo, K. Samatha, V. Veeraiah, Phys. B: Condens. Matter 534 (2018)134-140.

[6] Min Ji Hyun, Woo Mi-Kyung, Yoon Ha Young, Jang Jin Woo, Wu Jun Hua, Lim Chae-Seung, et al. Anal Biochem 2014;447:114–8.

[7] Drmota A, Koselj J, Drofenik M, Znidarsic A. J Magn Magn Mater 2012;324:1225–9.

[8] B.D. Cullity, (1956), Elements of X-ray diffraction, Addison Wesley Publication reading, M.A.

[9] Costa ACFM, Leite AMD, Ferreira HS, Kiminami RHGA, Cavac S, Gama L. J Eur Ceram Soc 2008;28:2033–7.

[10] A. Nlebedim, K.W. Dennis, R.W. McCallum, D.C. Jiles, J. Appl. Phys. 115 (2014) 17A519.

[11] James V, Rao PP, Sameera S, Divya S. Ceram Int 2014;40(Issue 1 Part B):2229–35.

[12] Netto CGCM, Toma HE, Andrade LH. J Mol Catal B Enzym 2013;85–86:71–92.

[13] Guo F, Fang Z, Xu CC, Smith Jr RL. Prog Energy Combust Sci, Oxford, Inglaterra, GB 2012;38 (5):672–90.

[14] Jing H, Wang X, Liu Y, Wang A. Chin J Catal 2015;36(2):244–51.

[15] Akhtar MN, Khan MA, Ahmad M, Nazir MS, Imran M, Ali A, et al. J Magn Magn Mater 2017;421:260–8.

[16] Ambursa MM, Ali TH, Lee HV, Sudarsanam P, Bhargava SK, Hamid SBA. Fuel 2016;180:767–76.

[17] Li Y, Zhang C, Liu Y, Tang S, Chen G, Zhang R, et al. Fuel 2017;189:23–31.

[18] Jain SR, Adiga KC, Verneker VP. Combust Flame 1981;40:71–9.

[19] Klung H, Alexander L. New York: Wiley; 1962.

[20] N. Murali, S. Margarette, G.P. Kumar, B. Sailaja, S.Y. Mulushoa, P. Himakar, B.K. Babu, V. Veera iah, Phys. B Condens. Matter, 522 (2017) 1-6

[21] Reed JS. New York: John Wiley & Sons; 1996.